Rotation state evolution of retired geosynchronous satellites

Conor J. Benson and Daniel J. Scheeres
University of Colorado Boulder
429 UCB, Boulder, CO 80309

William H. Ryan and Eileen V. Ryan
Magdalena Ridge Observatory, New Mexico Institute of Mining and Technology
101 East Road, Socorro, NM 87801

Nicholas Moskovitz
Lowell Observatory
1400 W Mars Hill Road, Flagstaff, AZ, 86001

ABSTRACT

Non-periodic light curve rotation state analysis is conducted for the retired geosynchronous satellite GOES 8. This particular satellite has been observed periodically at the Maui Research and Technology Center as well as Magdalena Ridge and Lowell Observatories since 2013. To extract tumbling periods from the light curves, two-dimensional Fourier series fits were used. Torque-free dynamics and the satellite's known mass properties were then leveraged to constrain the candidate periods. Finally, simulated light curves were generated using a representative shape model for further validation. Analysis of the light curves suggests that GOES 8 transitioned from uniform rotation in 2014 to continually evolving tumbling motion by 2016. These findings are consistent with previous dynamical simulations and support the hypothesis that the Yarkovsky-O'Keefe-Radzievskii-Paddack (YORP) effect drives rotation state evolution of retired geosynchronous satellites.

1. INTRODUCTION

With the growing value of geosynchronous orbit for communications and observation, understanding the motion of defunct satellites in and near the geostationary belt is all the more important. Many of these satellites are known to have fast or evolving spin states [1,2,3]. Better understanding of the mechanisms driving retired satellite rotation state evolution promises a number of benefits. Knowledge of this motion will allow for the prediction of rapid spin rates capable of material shedding or satellite break-up. In addition, this knowledge will yield more accurate estimates for attitude dependent solar radiation forces for long-term orbit prediction. Finally, most proposed on-orbit debris mitigation and servicing/recycling missions require physically restraining or grappling potentially tumbling, non-cooperative target satellites. While designing and executing such missions, accurate predictions of the target's evolving rotation state will be invaluable.

Albuja et al. hypothesize that the observed evolution of some defunct satellites is largely driven by the Yarkovsky-O'Keefe-Radzievskii-Paddack (YORP) effect, a phenomenon in which the absorption, reflection and delayed re-emission of solar radiation generate torques on an orbiting body [4]. Through dynamical simulations, Albuja et al. showed that YORP theory closely predicts the observed rotation period evolution of the retired GOES 8 and GOES 10 satellites [5]. Between December 2013 and July 2014, the observed rotation period of GOES 8 increased from 16.83 s to 75.66 s [2,3]. The Albuja et al. simulations also suggested a continued increase in GOES 8's rotation period resulting in a transition to non-principal-axis (tumbling) motion [5,6]. Photometric light curves of GOES 8 taken by Ryan & Ryan in September 2015 and February 2016 seemed to confirm this transition as the observations did not exhibit clear periodicity [3,6]. Given these findings and the simulation results, Albuja et al. hypothesize that GOES 8 and other retired satellites cycle between phases of uniform and tumbling motion due to the competing influences of YORP and kinetic energy dissipation [6]. As a satellite's spin rate approaches zero due to YORP, it loses its angular momentum and begins to tumble. According to Albuja et al., the satellite then spins up

preferentially about its axis of minimum inertia since this axis requires the minimum torque to accelerate. While spinning up about this axis, energy dissipation starts to dominate. This eventually causes the satellite to return to stable uniform rotation about the axis of maximum inertia. With all excess energy dissipated, YORP again becomes the most dominant perturbation and the cycle starts over [6].

The following work will explore this cyclic hypothesis by analyzing several non-periodic optical light curves of GOES 8 obtained between September 2015 and July 2016. Using frequency analysis and leveraging rigid body dynamics, as well as shape and mass distribution information about GOES 8, plausible tumbling rotation states are extracted from each light curve to gain insight into how the satellite is evolving.

2. OBSERVATIONS

GOES 8 has been observed several times at Magdalena Ridge Observatory (Socorro, NM) and Lowell Observatory (Flagstaff, AZ) between September 2015 and July 2016. All Magdalena Ridge Observatory (MRO) observations were taken using the observatory's 2.4 m telescope fitted with an Andor iKon 936 CCD camera and Bessel VR filter. Images were taken at a rate of 1-2 Hz with the exposure time adjusted for each arc based on satellite brightness. Photometric data were obtained from the resulting images using the IRAF *phot* task, yielding instrumental magnitudes only. Single data points with clear contamination from field stars were removed. Given the fast sampling cadence and relatively large sidereal tracking rates, it was unlikely for a field star to contaminate several consecutive images. So peak features with several or more data points were taken as satellite glints. Reference [3] provides additional details about the instruments, data collection and reduction. The MRO light curves are plotted in Fig. 1-2 along with the initial and final observer-satellite-sun phase angles for each arc. Fig. 1 shows the 12 Sept 2015 GOES 8 light curve consisting of two segments separated by approximately 35 minutes. Upon initial inspection, it is unclear if the satellite is tumbling given the earlier segment alone. The later segment on the other hand clearly lacks defined periodicity.

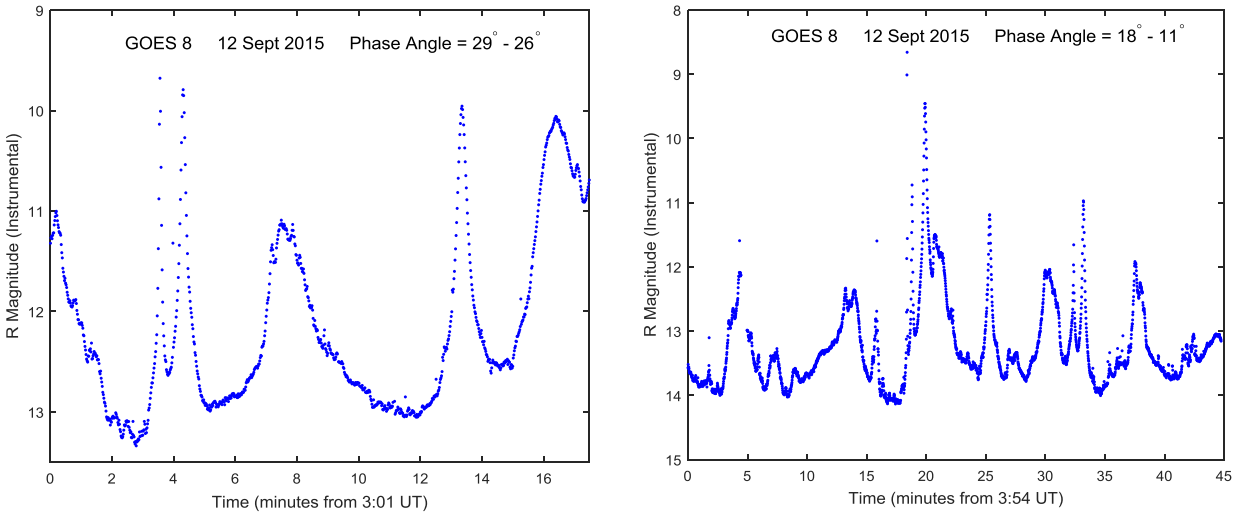

Fig. 1. 12 Sept 2015 GOES 8 Light Curves

The 6 Feb 2016 light curve, plotted in Fig. 2, shows more structure than the previous one. On closer inspection though, the aperiodic glint features and uneven peak spacing again suggest tumbling motion. This becomes more apparent when the light curve is phase folded [2]. The smallest dispersion was found for a folded period of 13.64 min. Even for this best-fitting case, the folded light curve, plotted in Fig. 2, shows significant peak dispersion. Previous GOES 8 observations show minimal dispersion for uniform rotation, even for large changes in solar phase angle (~17°) [2].

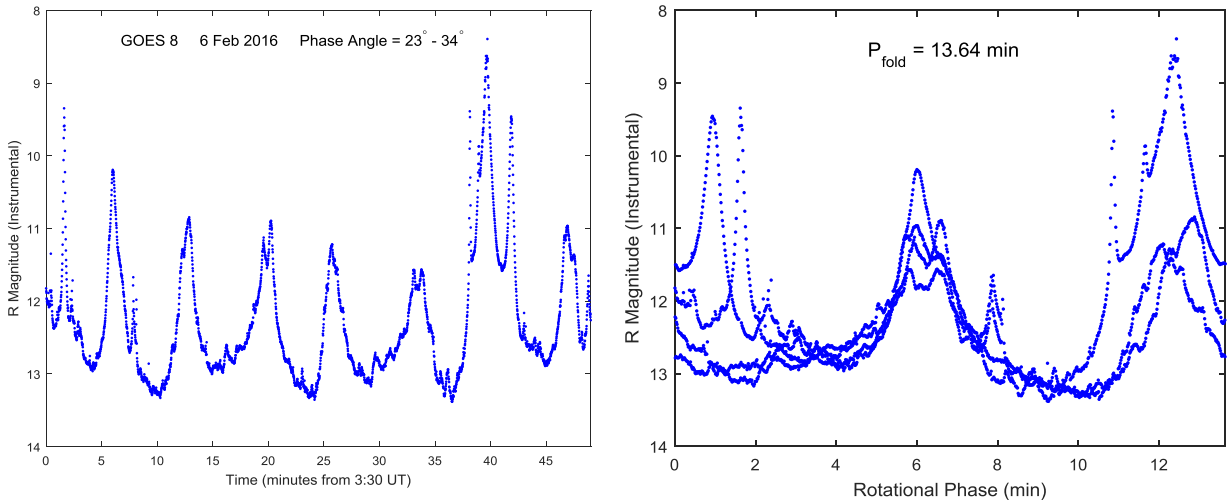

Fig. 2. Left: 6 Feb 2016 Light Curve Right: Folded 6 Feb 2016 Light Curve

The 3 Jul 2016 observations were taken using Lowell Observatory's 1.1 m Hall telescope fitted with an EV2 CCD231 CCD camera and VR filter. Images were taken with 1 s exposures at a cadence of 11 s, the majority of which was required for CCD readout. The images were reduced using IRAF and a custom IDL pipeline. The magnitudes were then calibrated against the 2MASS star catalogue to remove atmospheric extinction effects. As before, data contaminated by field stars was removed. Reference [7] provides added details on the instruments, data collection, and reduction for the Lowell Observatory light curves. The 3 Jul 2016 light curve is shown in Fig. 3. Repointing was required due to the use of constant rate tracking, resulting in a ~5 min observation gap. In spite of this gap and the relatively low sampling rate, the light curve clearly does not exhibit defined periodicity.

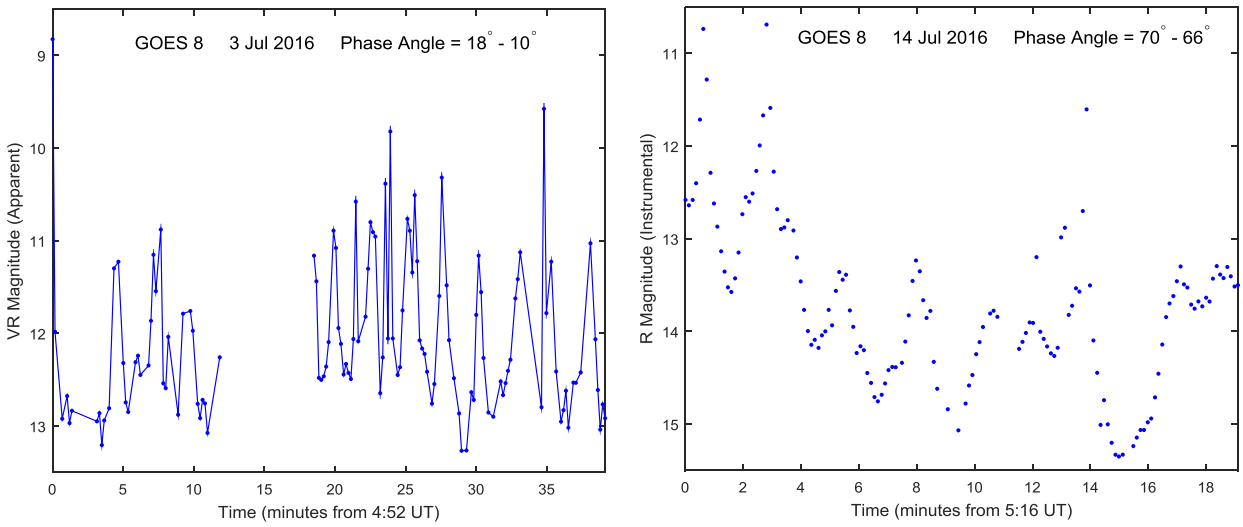

Fig. 3. Left: 3 Jul 2016 Light Curve Right: 14 Jul 2016 Light Curve

The 14 July, 2016 observations were taken using Lowell's 1.8 m Perkins telescope fitted with the PRISM 2048×2064 pixel CCD camera and R filter. As before, images were taken with 1 s exposures but at a faster cadence of 7 s. The reduction process was the same as for the 3 Jul 2016 observations except that only instrumental magnitudes were obtained. The 14 Jul 2016 light curve is also plotted in Fig. 3. With the 1.8 m Perkins' higher sampling cadence, more details are visible in the light curve. As with the light curve from two weeks prior, there is no defined periodicity. An interesting feature in the 14 Jul 2016 light curve is the rapid drop in mean magnitude over time. Given that the solar phase angle changed by only 4° during the arc, this drop is likely driven more by the

satellite's rotation than varying lighting geometry. When compared with the 6 Feb 2016 light curve, the two from July have significantly higher frequencies, suggesting an increase in the satellite's spin rate over this timespan.

3. METHODOLOGY

3.1 Tumbling Fundamental Periods

With the September 2015 – July 2016 GOES 8 light curves all demonstrating complex tumbling motion, methods for extracting plausible tumbling rotation states from these light curves will now be discussed. Considering that observed changes in GOES 8's uniform rotation period occurred at much longer time scales than a typical observation arc (<1 hr), it will be assumed that the satellite's motion can be well-approximated by torque-free rigid body dynamics for the duration of a given light curve. Under torque-free rigid body assumptions, the tumbling motion of a body is described by two fundamental periods [8]. There are several common conventions for defining these two fundamental periods, all based on Euler angle sets. The long axis convention used in this analysis is shown in Fig. 4. For torque-free dynamics, the magnitude and direction of the satellite's rotational angular momentum vector $\vec{\boldsymbol{H}}$ are constant. So this vector provides a convenient reference for the satellite's motion. With the satellite's axis of minimum inertia (often its longest axis) initially aligned with $\vec{\boldsymbol{H}}$, the satellite body frame is sequentially rotated through the angles ϕ, θ, and ψ according to the 3-1-3 Euler angle set [8]. So with this long axis convention, $P_{\bar{\phi}}$ is the average precession period of the long axis about $\vec{\boldsymbol{H}}$ and P_{ψ} is the rotation period of the long axis about itself. The nutation period P_{θ} is always proportional to P_{ψ}, so only $P_{\bar{\phi}}$ and P_{ψ} are independent [9]. Therefore, $P_{\bar{\phi}}$ and P_{ψ} are called the fundamental tumbling periods. $P_{\bar{\phi}}$ and P_{ψ} in a chosen convention can be uniquely calculated for a given body with angular momentum H and rotational kinetic energy T [8,10]. Therefore, $P_{\bar{\phi}}$ and P_{ψ} are equivalent to H and T for describing the satellite's tumbling state. Another convenient convention, the short axis convention, is defined where $P_{\bar{\phi}}$ and P_{ψ} instead correspond to the precession and rotation of the satellite's maximum inertia axis (often a body's shortest dimension) about $\vec{\boldsymbol{H}}$,. One can easily transform between periods given in the short and long axis conventions [9].

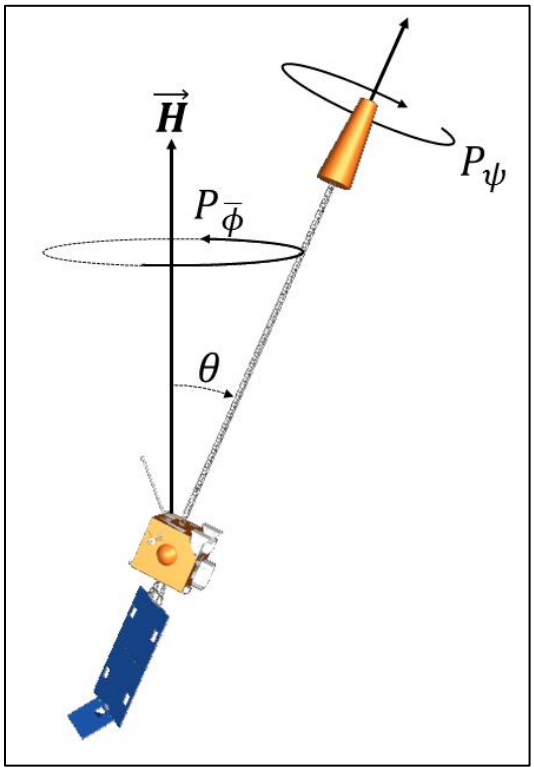

Fig. 4. Long Axis Convention Fundamental Periods with GOES Satellite

3.2 Two-Dimensional Fourier Series

Generally, the frequencies present in a tumbling light curve are linear combinations of the fundamental frequencies $f_{\bar{\phi}} = 1/P_{\bar{\phi}}$ and $f_{\psi} = 1/P_{\psi}$ [9,11,12]. Therefore the time-varying brightness $B(t)$ of a tumbling light curve can be modeled using a two-dimensional Fourier series,

$$B(t) = C_0 + \sum_{j=1}^{m}\left[C_{j0}\cos 2\pi j f_1 t + S_{j0}\sin 2\pi j f_2 t\right] + \sum_{k=1}^{m}\sum_{j=-m}^{m}\left[C_{jk}\cos 2\pi(jf_1 + kf_2)t + S_{jk}\sin 2\pi(jf_1 + kf_2)t\right]$$

Here, f_1 and f_2 are the fundamental frequencies, m is the Fourier series order, C_0 is the mean light curve brightness, and (C_{jk}, S_{jk}) are the coefficients associated with each linear combination of f_1 and f_2 [12]. This Fourier series model assumes that the brightness variation is driven solely by the satellite's rotation with fixed lighting and viewing geometry. Therefore, it will only approximate real satellite light curves since time-varying solar phase angles and synodic vs. sidereal spin rates also influence the observed brightness variation.

To extract the fundamental periods from a tumbling light curve, one can search a grid of potential period pairs. For each pair, a two-dimensional Fourier series of order m is fit to the observations using a least squares method. The goal is to find the period pair yielding the best fit to the observations (i.e. the lowest residual). There are a number of issues with this approach though. First of all, several different period pairs often fit the light curve well. Also, the fitting process provides no information about which of the two periods $P_1 = 1/f_1$ and $P_2 = 1/f_2$ correspond to $P_{\bar{\phi}}$ and P_{ψ}. Finally, a given ($P_{\bar{\phi}}$, P_{ψ}) pair can describe both a long axis mode (LAM) and short axis mode (SAM) tumbling state. For LAM states, $\vec{\boldsymbol{H}}$ precesses about the axis of minimum inertia. For SAM states, $\vec{\boldsymbol{H}}$ precesses about the axis of maximum inertia [13]. Furthermore, being closer to uniform rotation about the maximum inertia axis (minimum energy state), SAMs have lower energy than LAMs. Therefore, a satellite in LAM experiencing energy dissipation will be driven through the SAM regime towards uniform rotation about the maximum inertia axis. Returning to periods assignments, a (P_1,P_2) pair could correspond to any of four possible tumbling states.

3.3 Moment of Inertia Constraints

One way to constraint the possible periods is to leverage moment of inertia information about the satellite. Only some ($P_{\bar{\phi}}$, P_{ψ}) pairs are physically possible for given moments of inertia [8,9,10,11]. If the satellite's moments of inertia are known, each of the four candidate period assignments can be tested for viability. Fortunately, GOES 8's end of life moments of inertia are known [5]:

$$[I]_{GOES\,8} = \begin{bmatrix} I_l & 0 & 0 \\ 0 & I_i & 0 \\ 0 & 0 & I_s \end{bmatrix} = \begin{bmatrix} 980.5133 & 0 & 0 \\ 0 & 3440.9438 & 0 \\ 0 & 0 & 3561.0894 \end{bmatrix} kg\ m^2$$

Following the conventions described earlier, I_l, I_i, and I_s are the satellite's minimum, intermediate, and maximum moments of inertia respectively. Using these known moments of inertia, plots of viable $P_{\bar{\phi}}$ and P_{ψ} pairs for GOES 8 rotation states can generated. Two such plots are provided in Fig. 5. Here, $P_{\bar{\phi}}$ and P_{ψ} are given in the conventions most consistent with the rotation state, long axis for LAMs and short axis for SAMs. Impossible period pairs are denoted by the white regions. Also included in the plot is the average or minimum long axis nutation angle θ for each viable period pair [8]. The closer θ is to 0°, the closer the satellite is to uniform rotation about its long axis (the maximum energy state for a given angular momentum H). The closer θ is to 90°, the closer to uniform rotation about the axis of maximum inertia (the minimum energy state for a given H). Fig. 5 shows that many more period pairs are viable for LAMs than SAMs. This is due to GOES 8's nearly prolate moments of inertia, $I_s \approx I_i > I_l$. These inertia constraints will be leveraged when analyzing the observations.

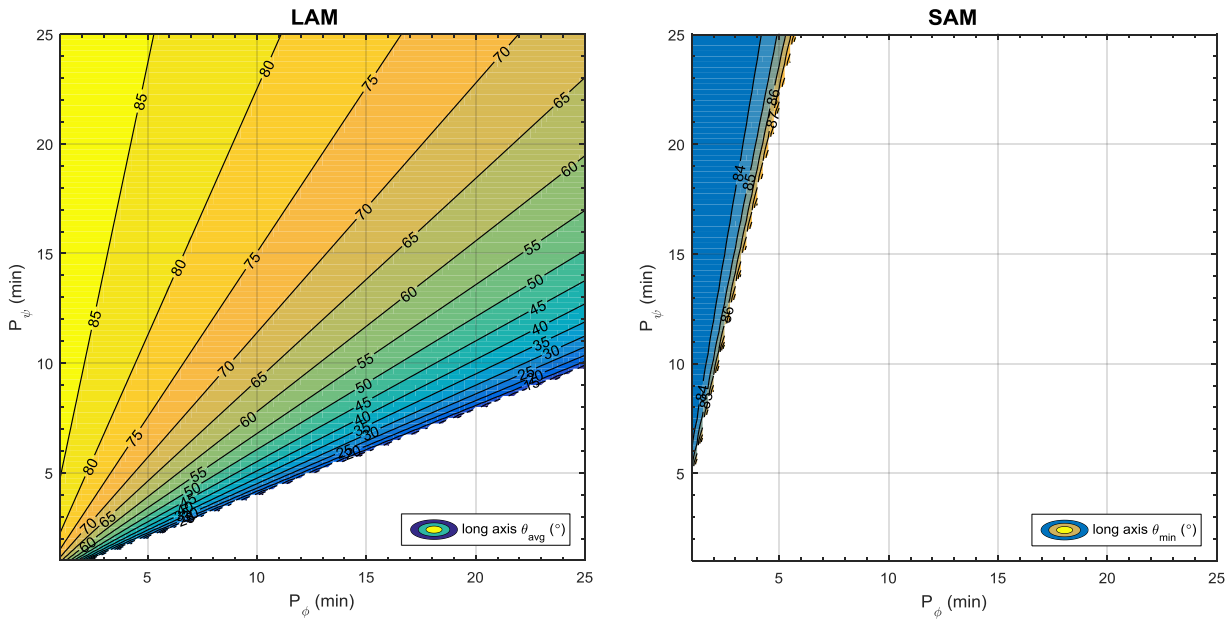

Fig. 5. Viable GOES 8 Tumbling Period Pairs and Corresponding Long Axis Nutation Angles

3.4 Simulated Light Curves

Unfortunately, there are often several viable tumbling states remaining after the moment of inertia constraints are applied. At this point, a logical option is to generate simulated light curves for each of the possible tumbling states using a representative model of the satellite and compare them with the observations. Given the complexity of the observed tumbling light curves, a light curve simulator is desired that can accurately model specular, glossy, and diffuse reflections as well as shadows and indirect illumination (i.e. multiple reflections). So a satellite light curve simulator was created from an existing stochastic ray tracer developed by NASA Goddard Space Flight Center (GSFC). A detailed GOES 12 shape model was also available for use. Given that the GOES 8 through GOES 12 satellites are nearly identical, the shape model can be used to represent any of them [14]. This shape model's optical properties are defined by a micro-facet bidirectional reflectance distribution function (BRDF) capable of creating glossy as well as specular and diffuse reflections with different optical parameters for each surface material. To facilitate comparison with specific observations, the correct time-varying positions of the satellite, sun, and earth-based observer were accounted for. The satellite's orbit was propagated from two line element (TLE) data obtained from the Joint Space Operations Center's Space-Track database. JPL ephemerides were used to determine the sun's position and earth's rotation. Finally, WGS 84 coordinates were used for the observation sites (i.e. MRO or Lowell Observatory). A sample ray traced image of the GOES shape model is shown in Fig. 6. This image illustrates the diverse reflections and complex shadowing possible with the NASA GSFC ray tracer. From the ray traced images, the satellite's brightness was determine by summing the radiance values over all pixels in the image and multiplying by constant pixel solid angle. This yielded a total irradiance at the camera focal point, taken as the measured brightness. For this model, atmospheric extinction and a telescope model were not considered. As a result, only relative magnitudes were used to compare the simulated and observed light curves.

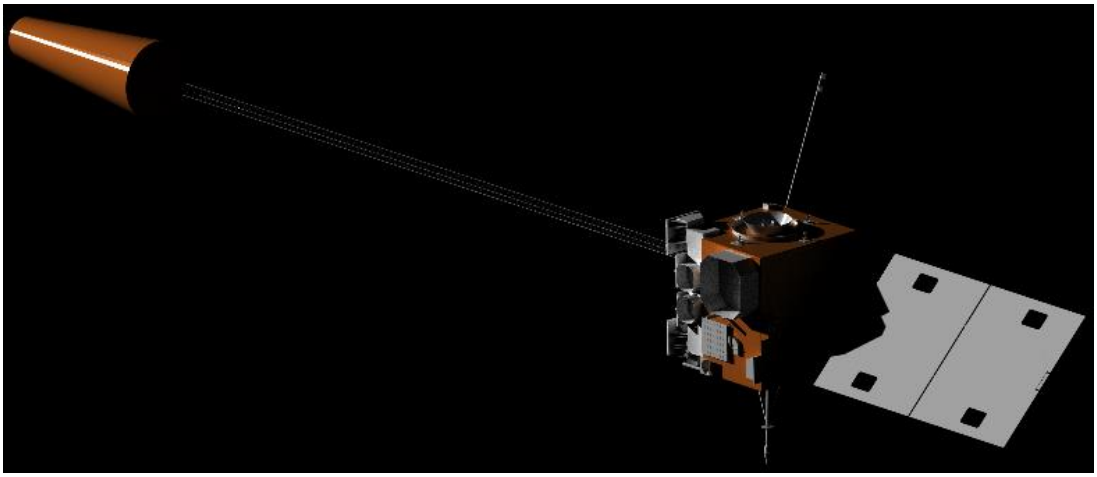

Fig. 6. Ray Traced Image of GOES Shape Model

3.5 Test Case

To test the Fourier series analysis methods presented earlier, simulated observations were generated using the GOES shape model with a known tumbling rotation state. For this test case, a LAM rotation state with long axis convention periods $P_{\bar{\phi}} = 14.52$ min and $P_{\psi} = 12.27$ min was prescribed. Also, the initial epoch was made the same as for the 6 Feb 2016 GOES 8 observations with the observer located at MRO for realistic sun-satellite-observer geometry. The resulting light curve is provided in Fig. 7. This light curve features several prominent glints and complex structure. Also visible is a trend towards decreasing magnitudes over time. This is due to the time-varying phase angle. To gain insight about the light curve's frequency structure, its Fourier transform is also provided in Fig. 7. The Fourier transform shows that all of the light curve's prominent frequencies are low order linear combinations of the two fundamental frequencies [9,11].

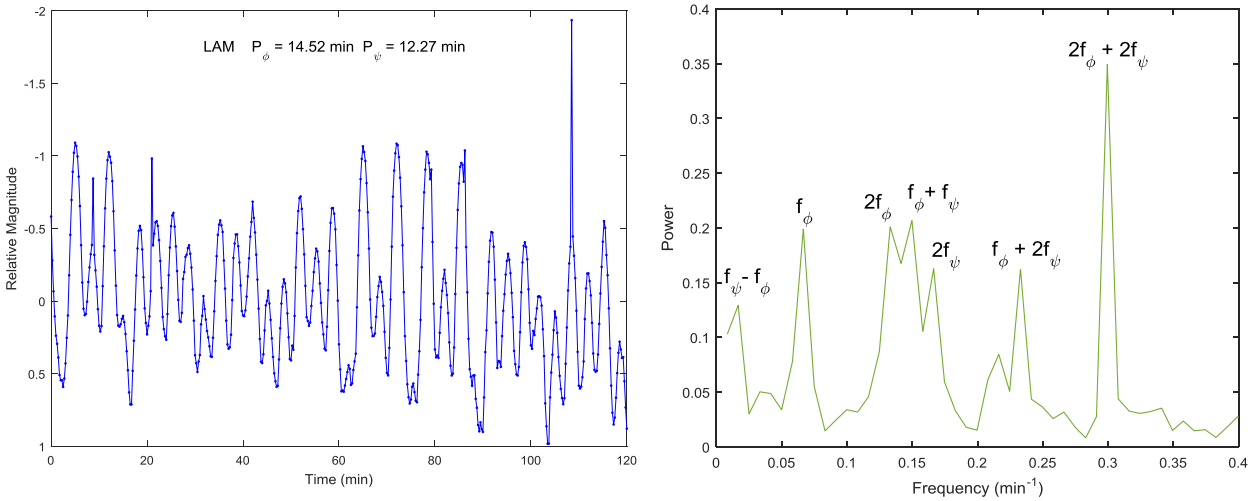

Fig. 7. Simulated GOES 8 Tumbling Light Curve and Corresponding Fourier Transform

Now, two-dimensional Fourier series can be fitted to the light curve for various period pairs to determine whether this method can successfully extract the two fundamental periods. For this test case, only the first 60 min of the Fig. 6 light curve were used to limit the change in phase angle (still a ~15° change). Given that all prominent peaks in the Fig. 7 Fourier transform are order two or less, the two-dimensional Fourier series was truncated at $m = 2$. Searching over a square grid with periods ranging from 2 – 30 min and 5 s spacing, the resulting root mean square (RMS) residual value for each period pair is shown in Fig. 8. Here only the lower diagonal is shown since the upper

diagonal will just be a reflection of these values over the line $P_1 = P_2$. The plot shows that a small subset of the period pairs (those in dark blue) fit the light curve significantly better than the rest.

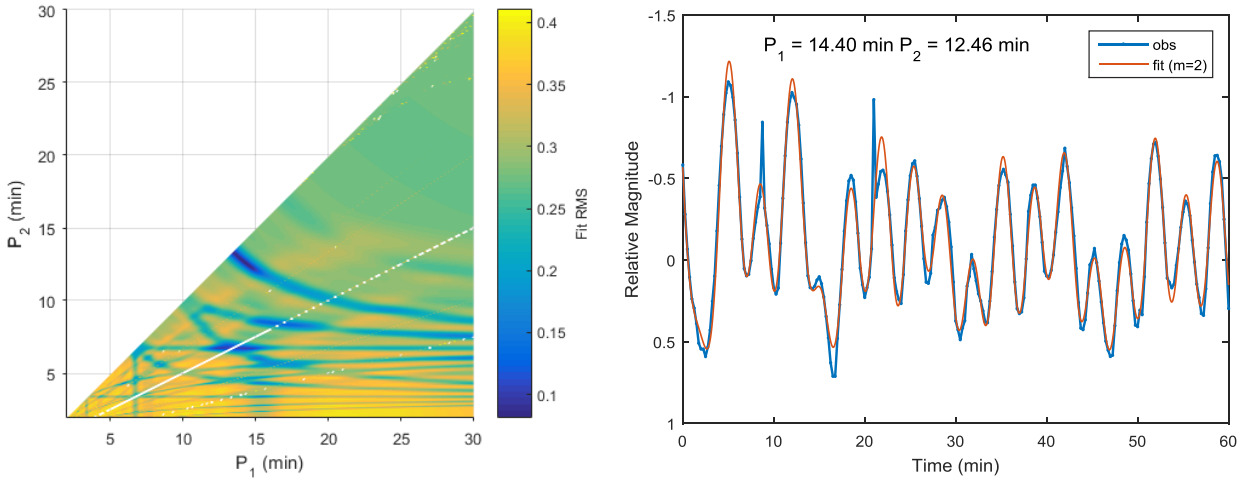

Fig. 8. RMS Residuals for Fourier Series Fits to Simulated GOES 8 Light Curve ($m = 2$) and Best Fit

Finding the local minimum of each dark blue basin with a linearized/iterative least squares algorithm, the best fitting period pairs were found to be: 1) $P_1 = 12.47$ min $P_2 = 6.69$ min, 2) $P_1 = 14.41$ min $P_2 = 6.67$ min, and 3) $P_1 = 14.40$ min $P_2 = 12.46$ min. It is important to note that $1/6.68 \cong 1/14.40 + 1/12.46$. So the frequencies corresponding to these three well-fitting periods are linearly related. Given this relationship, it is easy to see why all three pairs fit similarly well, as the terms in their respective Fourier series will have many of the same frequencies. Determining the correct period pair and which of the four possible tumbling states it represents requires applying the moment of inertia constraints and generating simulated light curves to see which state best replicates the observed light curve structure. At this point, it is important to note that $P_1 = 14.40$ min $P_2 = 12.46$ min pair fits the light curve slightly better than the other two pairs and is almost equal to the prescribed pair. The Fourier series fit for $P_1 = 14.40$ min $P_2 = 12.46$ min is shown in Fig. 8 and closely matches the observations. The discrepancy between this pair and the truth is likely due to the time-varying phase angle. Nevertheless, these observed periods differ from the true periods by less than 2%. This demonstrates that while simple, two dimensional Fourier series fits can provide reasonable estimates for the fundamental periods, even if the observations span a significant range of phase angles (~15° for this test case).

4. ANALYSIS

The preceding methods for extracting tumbling rotation states and constraining the possible solutions will now be applied to the non-periodic GOES 8 light curves. In the following analysis unless otherwise specified, LAM states will be described in the long axis period convention and SAM states in the short axis convention. This approach is consistent with conventions for the moment of inertia constraints in Fig. 5.

4.1 12 September 2015

Given that the 12 Sept 2015 observations are in two segments (a,b) with a ~35 min observation gap and significant change in mean magnitude (likely due to the phase angle change), they will be analyzed separately. Nevertheless, dynamical changes to the satellite's fundamental periods should be negligible over the combined observation arc. So at least one particular period pair should fit both segments well. Segment (a) contains relatively few peaks, resulting in an overwhelming number of similarly good fits. So segment (b) was analyzed first before returning the former. The Fourier series grid search with $m = 2$ for segment (b) is shown in Fig. 9. Several pairs yield significantly better fits to the light curve than the rest. The four best fitting pairs are provided in Table 1. As with the test case above, these pairs' frequencies are all linearly related. The pair P_1 = 6.70 min and P_2 = 16.69 min provides a slightly better fit than the other three. Fits for this pair to both 12 Sept 2015 segments are included in Fig. 10. In these plots, the fit

peaks align well with the general light curve variability. Glints and higher frequency features require a higher Fourier series order to replicate. Here it should be noted that the number of Fourier series coefficients C_0, C_{jk}, and S_{jk} goes as $(2m+1)^2$. With significantly more degrees of freedom, higher order expansions generally yield better fits at the expense of many more well-fitting solutions to choose between. As illustrated in the test case above, most prominent light curve frequencies are low order ($m \leq 2$) linear combinations of $f_{\bar{\phi}}$ and f_{ψ}. So second order ($m = 2$) fits are usually sufficient to model the major light curve structure.

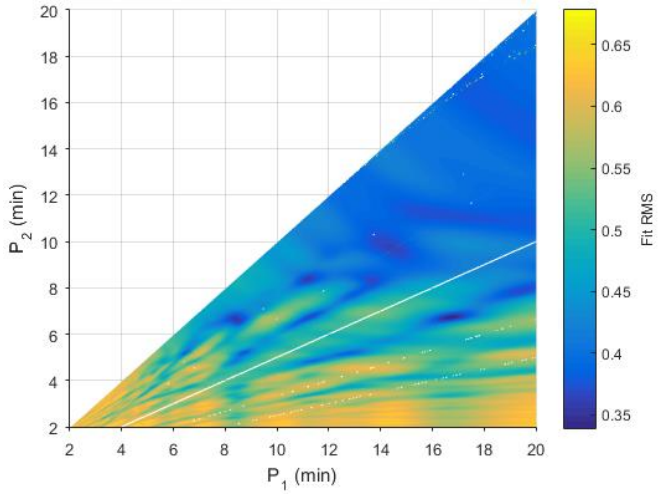

Fig. 9. 12 Sept 2015 (b) 2-D Fourier Series RMS Residuals ($m = 2$)

Table 1. 12 Sept 2015 (b) Best Fit Periods

Pair	P_1 (min)	P_2 (min)	Fit RMS
1	6.66	8.33	0.350
2	6.71	11.23	0.363
3	6.70	16.69	0.336
4	8.36	11.17	0.353

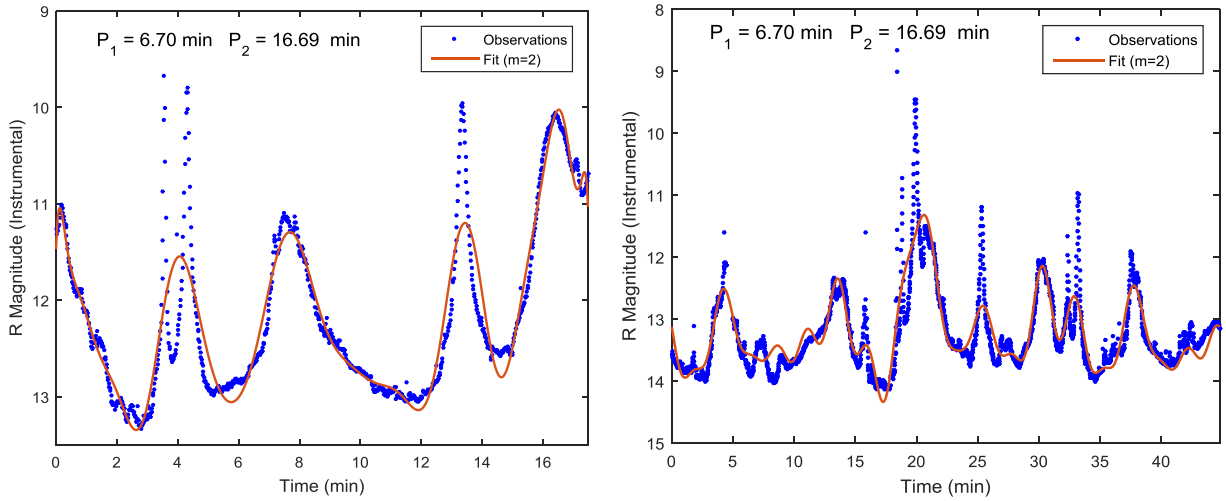

Fig. 10. 12 Sept 2015 (a,b) Best Fit

To help narrow down the 16 candidate rotation states in Table 1 (two LAM and two SAM for each pair), moment of inertia constraints will be applied. For short axis convention SAM periods, $P_{\psi}/P_{\bar{\phi}} > 2$ for all real bodies [9]. This constraint immediately eliminates seven of the eight candidate SAM states from Table 1. Unfortunately, long axis convention LAM periods do not have an equally useful general constraint [8]. Leveraging GOES 8's particular moments of inertia, the remaining candidate states are analyzed using Fig. 5. First of all, these plots show that the

final candidate SAM state is not possible for GOES 8. Unfortunately, the GOES 8 inertia constraints do not reduce the possible LAM states in this case. Nevertheless, Fig. 5 shows that θ_{avg} for these states will be quite different. For the two LAM states corresponding to period pair 3, θ_{avg} is 14° and 81° respectively. Overall, given that pair 3 fits the observations best, the most plausible rotation states for the 12 Sept 2015 light curve are LAM with $P_{\bar{\phi}} = 6.70$ min $P_{\psi} = 16.69$ min or $P_{\bar{\phi}} = 16.69$ min $P_{\psi} = 6.70$ min.

4.2 6 February 2016

The results of the period grid search for the 6 Feb 2016 GOES 8 observations are provided in Fig. 11. Interestingly, one region with the local minimum, P_1 = 12.28 min and P_2 = 14.50 min, clearly provides a superior fit to all others. The $m = 2$ fit for this pair, included in Fig. 11, closely matches the general structure of the observed light curve.

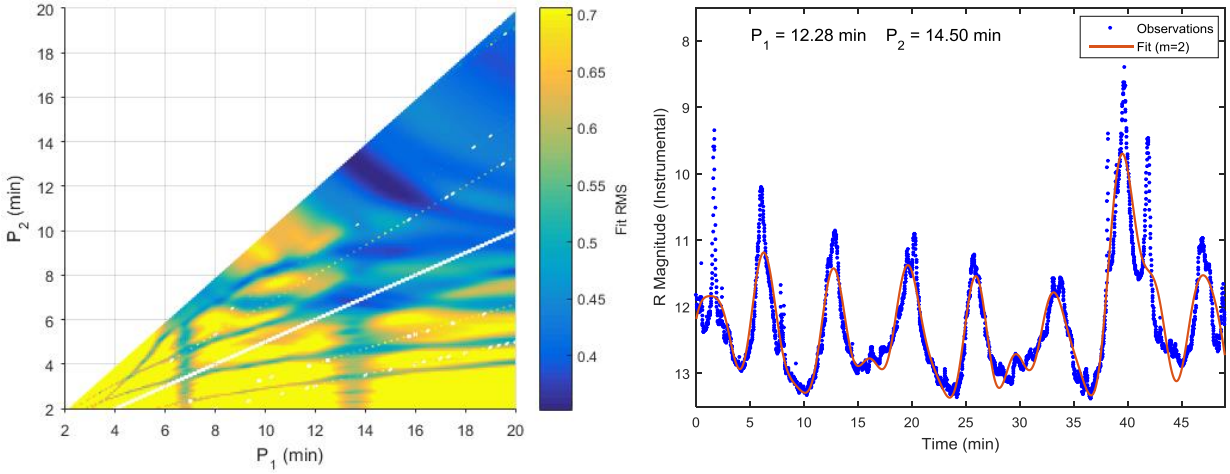

Fig. 11. 6 Feb 2016 2-D Fourier Series RMS Residuals and Best Fit ($m = 2$)

Applying the moment of inertia constraints, neither SAM state is possible given the $P_{\psi}/P_{\bar{\phi}} > 2$ requirement, but both LAM states are still possible. To hopefully determine the correct LAM state, simulated light curves were generated with a coarse search over possible initial attitudes and angular velocity phasing. This search yielded the following results shown in Fig. 12. It should be noted that the true solar array orientation for GOES 8 is unknown. In addition, the shape model reflective properties likely differ from the truth. So simulated light curves generated with the current shape model cannot be expected to match all observed features. Nevertheless, both LAM states yield light curves with similar amplitude and frequency to the observations, with the $P_{\bar{\phi}} = 14.50$ min $P_{\psi} = 12.28$ min fit having noticeably better alignment with the major peaks. Even when the amplitudes differ significantly at the large glint around 40 min, the peaks are aligned. On the other hand, the $P_{\bar{\phi}} = 12.28$ min $P_{\psi} = 14.50$ period assignment yields peaks that are slightly off in frequency. These findings suggest that $P_{\bar{\phi}} = 14.50$ min $P_{\psi} = 12.28$ min is the more plausible assignment. Nevertheless, both states are ultimately quite similar from the perspective of the overall evolution with θ_{avg} for LAM $P_{\bar{\phi}} = 14.50$ min and LAM $P_{\bar{\phi}} = 12.28$ min being 63° and 71° respectively.

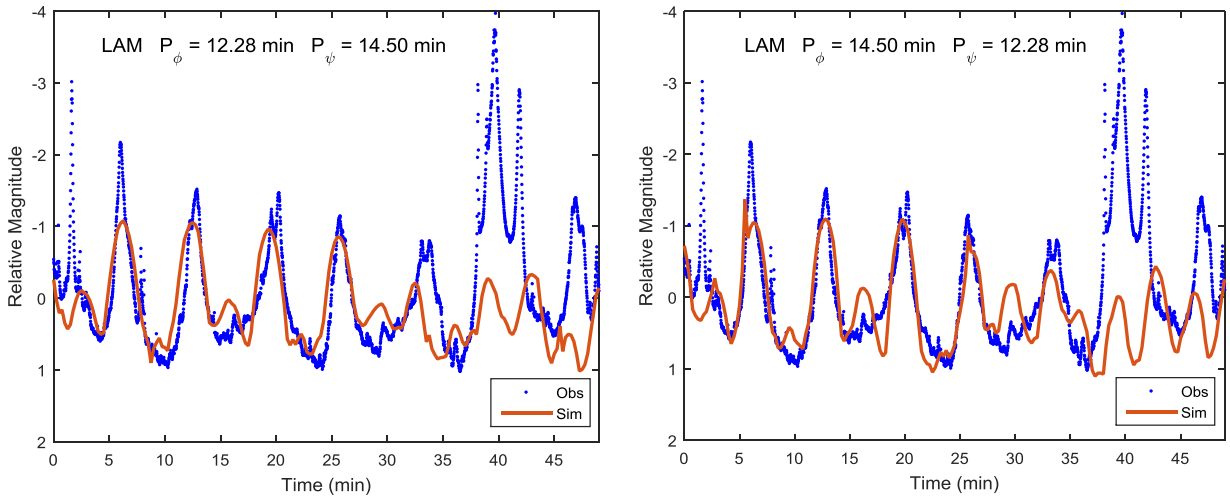

Fig. 12. Observed and Simulated 6 Feb 2016 GOES 8 Light Curves

4.3 3 July 2016

The two-dimensional Fourier series grid search results for the 3 Jul 2016 GOES 8 light curve are plotted in Fig. 13. There is a small region centered on $P_1 = 3.66$ min $P_2 = 8.61$ with significantly better fits. The best fit light curve for these periods is shown in the right plot of Fig. 13. Although the observations are sparse and a significant gap is present, the fit closely matches all major variations (the flat segment in the observations at ~2 min is due to contaminated points that were removed).

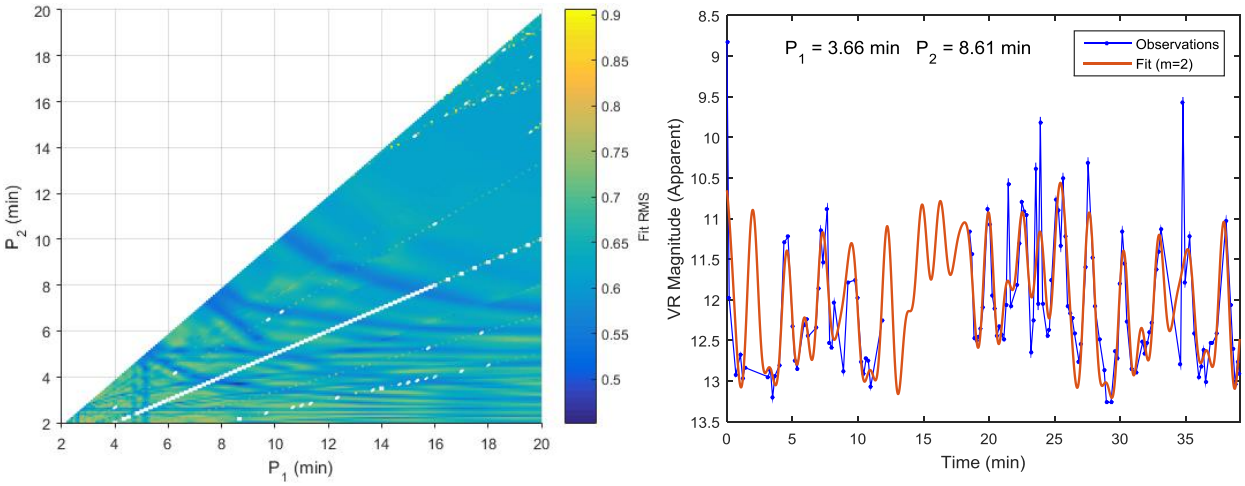

Fig. 13. 3 Jul 2016 2-D Fourier Series RMS Residuals and Best Fit (m =2)

Applying the moment of inertia constraints, neither SAM state is possible for GOES 8's nearly prolate moments of inertia. Both LAM states are possible though, with θ_{avg} for $P_{\bar{\phi}} = 3.66$ min and $P_{\bar{\phi}} = 8.61$ min being 80° and 24° respectively.

4.4 14 July 2016

The two-dimensional Fourier series grid search results for the 14 Jul 2016 GOES 8 light curve are plotted in Fig. 14. The first observation is that the majority of well-fitting pairs have one period of ~ 4 min. The large dispersion of well-fitting periods between 10 - 30 min is likely due to the short time-span of the light curve since longer arcs are needed to resolve longer periods. Overall, the pair with the lowest RMS residual for $m = 2$ is $P_1 = 3.95$ min $P_2 =$ 20.64 min. Another of the best-fitting pairs is $P_1 = 3.67$ min $P_2 =$6.67 min.

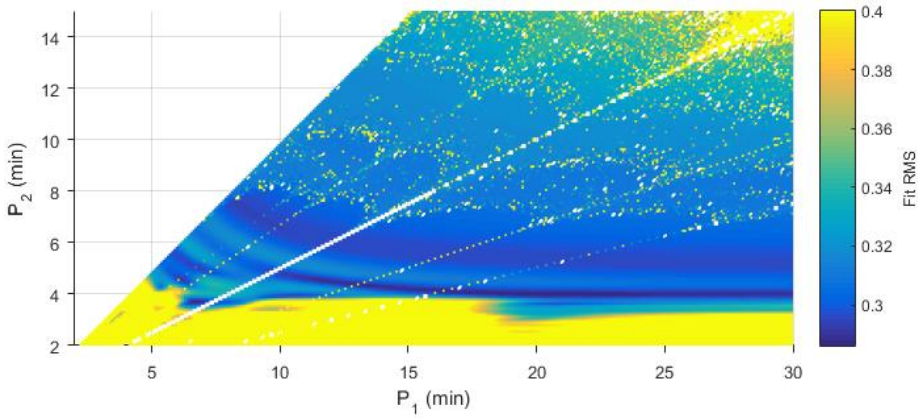

Fig. 14. 14 Jul 2016 2-D Fourier Series RMS Residuals ($m = 2$)

To compare these two period pairs, their fits are shown in Fig. 15. Here it is clear that $P_1 = 3.95$ min $P_2 = 20.64$ min fits the light curve more consistently, particularly at ~12 min. Applying moment of inertia constraints to this better-fitting pair, it was found that only SAM $P_{\bar{\phi}} = 3.95$ min $P_\psi = 20.64$ min and LAM $P_{\bar{\phi}} = 3.95$ min $P_\psi = 20.64$ min are possible. Form Fig. 5, these states both have $\theta \approx 85°$. Given how many well-fitting pairs exist along the dark blue region in Fig. 14 for $P_1 \approx 4$ min, other possible rotation states should be discussed. If a LAM is assumed with $P_{\bar{\phi}} \approx 4$ min, Fig. 5 shows that $\theta_{avg} > 80°$ for $P_\psi > 10$ min. So in terms of understanding overall evolution, LAM states with $P_{\bar{\phi}} \approx 4$ min and $P_\psi > 10$ min are all fairly flat spins. If the opposite LAM assignment is assumed with $P_\psi \approx 4$ min, Figs. 5 and 14 shows that the number of viable, well-fitting pairs is small. Only values of $P_{\bar{\phi}}$ between 10-12 min meet both criteria. These states will have relatively small nutation angles with $\theta_{avg} < 30°$. As for SAMs with $P_{\bar{\phi}} \approx 4$, Fig. 5 illustrates that changing P_ψ will not affect θ_{min} significantly, as all of these rotation states are nearly flat spins. In summary, the best-fitting rotation states for the 14 Jul 2016 light curve either have either large or small nutation angles.

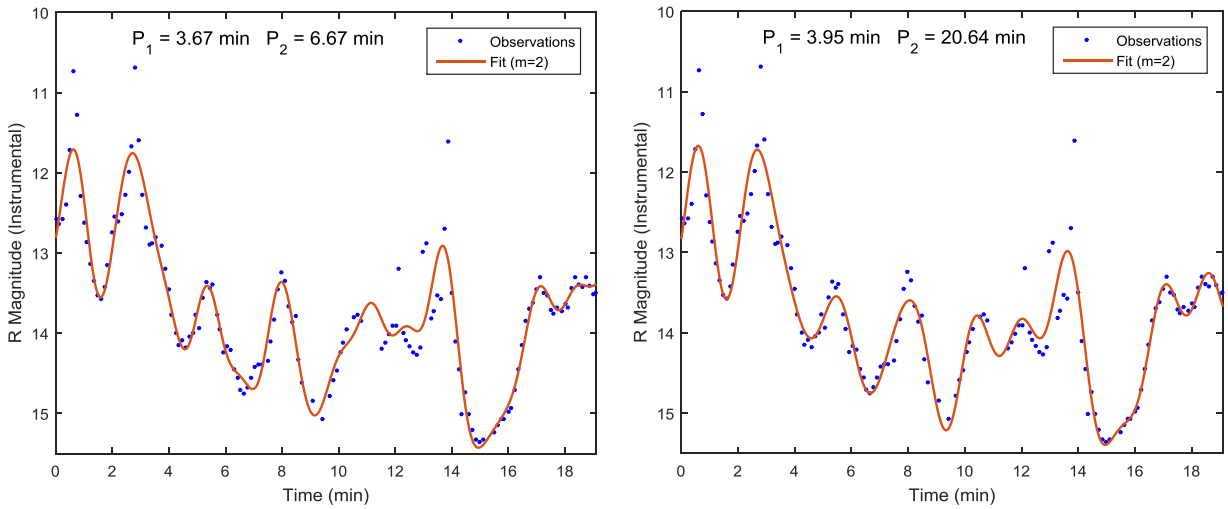

Fig. 15. 14 Jul 2016 GOES 8 Light Curve 2-D Fourier Series Fits

5. DISCUSSION

With plausible tumbling rotation states determined for GOES 8 at each epoch, they will now be discussed in the context of the GOES 8's historical and hypothesized evolution. Previous observations, provided in Table 2, show that the rotation period of GOES 8 increased significantly between late 2013 and mid 2014. As mentioned earlier,

YORP simulations by Albuja et al. predicted the rotation period to keep increasing, eventually leading to tumbling motion.

Table 2. GOES 8 Uniform Rotation Evolution

Date	Period
12 Dec 2013	16.83 s [2]
27 Feb 2014	16.48 s [2]
24 Apr 2014	22.95 s [3]
25 July 2014	75.66 s [2]

Summarizing the analysis of the previous section, plausible tumbling states for GOES 8 are provided in Table 3 along with the corresponding long axis nutation angle and long axis spin rate ω_l [8]. The strongest constraint on GOES 8's tumbling evolution was provided by the 6 Feb 2016 light curve, with LAM $P_{\bar{\phi}} = 14.50$ min $P_{\psi} = 12.28$ min yielding a clearly superior Fourier series fit as well as a simulated light curve consistent with the observations. To transition this far into the LAM regime from uniform rotation, the satellite would require significant spin up about its long axis. The LAM $P_{\bar{\phi}} = 6.70$ min state at the 12 Sept 2015 epoch is consistent with this spin up, with θ_{avg} decreasing and ω_l increasing. Considering now the two plausible 3 July 2016 solutions, both cases have significantly lower periods than for 6 Feb 2016 with higher ω_l. Again, a transition to either 3 Jul 2016 state would require additional long axis acceleration. Proceeding to 14 Jul 2016, the plausible LAM and SAM states both have higher nutation angles than for the 3 Jul 2016 states, indicative of more relaxed motion closer to uniform rotation.

Table 3. Plausible GOES 8 Tumbling Rotation States

Mode	$P_{\bar{\phi}}$ (min)	P_{ψ} (min)	Long Axis θ_{avg}	ω_l (rad/s)
12 Sept 2015				
LAM	6.70	16.69	81°	0.00991
LAM	16.69	6.70	14°	0.0217
6 Feb 2016				
LAM	14.50	12.28	63°	0.0120
3 Jul 2016				
LAM	3.66	8.61	80°	0.019
LAM	8.61	3.66	24°	0.0398
14 Jul 2016				
SAM	3.95	20.64	> 85°	0.00703
LAM	3.95	20.64	85°	0.0115

In all, while there are a number of possible evolutionary paths, the best-fitting rotation states do show a general trend. They suggest that GOES 8 transitioned from uniform motion to an excited long axis mode rotation state between 25 Jul 2014 and 6 Feb 2016 before returning to a more relaxed state closer to uniform rotation by 14 Jul 2016. This general trend would require the satellite's long axis spin rate to first increase then decrease, consistent with the Albuja et al. hypothesis that a tumbling GOES 8 will spin up preferentially about its long axis before energy dissipation drives it back towards the minimum energy state.

6. CONCLUSION

In an effort to better understand how the YORP effect may drive rotation state evolution of retired geosynchronous satellites, several non-periodic light curves of the retired GOES 8 satellite were analyzed. Leveraging torque-free rigid body dynamics, Fourier series frequency analysis, as well as known information about the satellite's shape and end of life moments of inertia, plausible tumbling rotation states were found at each observation epoch. Linking these plausible states together with previous observations suggests that GOES 8 evolved from uniform rotation into an excited tumbling state before transitioning back towards more relaxed motion. This apparent evolution agrees with the hypothesis that some retired geosynchronous satellites cycle between uniform and tumbling motion due to the combined influences of YORP and energy dissipation.

Given the complexity of these non-periodic light curves, more analysis is needed to further validate the plausible tumbling states at each observation epoch. This will require additional development of the light curve simulator to efficiently test many simulated light curves simultaneously. Hopefully by searching over smaller increments of initial attitude, angular velocity phasing, and solar panel orientation, close matches to the GOES 8 observations can be found. In all, this analysis only offers a glimpse into the evolution of one satellite. To truly understand and predict the rotation state evolution of GOES 8 and other retired geosynchronous satellites, more observations and dynamical modeling is needed.

7. ACKNOWLEDGEMENTS

The primary author would like to thank Steven Queen of NASA Goddard Space Flight Center for his assistance in developing the light curve simulator. In addition, this work was supported by a NASA Space Technology Research Fellowship.

8. REFERENCES

1. Papushev, P., Karavaev, Y., Mishina, M., Investigations of the evolution of optical characteristics and dynamics of proper rotation of uncontrolled geostationary artificial satellites, *Advances in Space Research*, Vol. 43(9), 1416–1422, 2009.
2. Cognion, R., Rotation rates of inactive satellites near geosynchronous earth orbit, *Proceedings of the 2014 Advanced Maui Optical and Space Surveillance Technologies Conference*, 2014.
3. Ryan, W.H., Ryan, E.V., Photometric Studies of Rapidly Spinning Decommissioned GEO Satellites, *Proceedings of the 2015 Advanced Maui Optical and Space Surveillance Technologies Conference*, 2015.
4. Albuja, A.A., Scheeres, D.J., McMahon, J.W., Evolution of angular velocity for defunct satellites as a result of YORP: An initial study, *Advances in Space Research*, Vol. 56(2), 237–251, 2015.
5. Albuja, A., Rotational Dynamics of Inactive Satellites as a Result of the YORP Effect, *Aerospace Engineering Sciences Graduate Theses & Dissertations (2015)*, 113, http://scholar.colorado.edu/asen_gradetds/113, retrieved Sept. 9, 2017.
6. Albuja, A.A., Scheeres, D.J., Cognion, R., Ryan, W.H., Ryan, E.V., The YORP Effect on the GOES 8 and GOES 10 Satellites: A Case Study, *Advances in Space Research*, (in review)
7. Benson, C.J., Scheeres, D.J., Moskovitz, N., Light curves of retired geosynchronous satellites, *Proceedings of the 7th European Conference on Space Debris*, 2017.
8. Samarasinha, N.L., A'Hearn, M.F., Observational and Dynamical Constraints on the Rotation of Comet P/Halley, *Icarus*, Vol. 93(2), 194-225, 1991.
9. Samarasinha, N.L., Mueller, B.E.A., Component periods of non-principal-axis rotation and their manifestations in the lightcurves of asteriods and bare cometary nuclei, *Icarus*, Vol. 248, 347-356, 2015.
10. Benson, C.J., Scheeres, D.J., Extraction and assignment of tumbling asteroid and defunct satellite rotation periods from simulated light-curve observations, *Proceedings of the 27th AAS/AIAA Space Flight Mechanics Meeting*, 2017.
11. Kaasalainen, M., Intepretation of lightcurves of precessing asteroids, *Astronomy and Astrophysics*, Vol. 376(1), 302-309, 2001.
12. Pravec, P. et al., Tumbling Asteroids, *Icarus*, Vol. 173(1), 108-131, 2005.
13. Landau, L.D., and Lifshitz, E.M., *Mechanics*, Vol. 1. Oxford, England: Pergamon Press, 2nd ed., 1969.
14. *GOES I-M Databook*, Rev. 1, Aug. 31, 1996, https://goes.gsfc.nasa.gov/text/goes.databook.html, retrieved Sept. 9, 2017.